Robust UAV Image Mosaicking Using SIFT and LightGlue

Sunghyeon Kim¹, Taejung Kim^{2*}

- ¹ Dept. of Smart City Engineering, Inha University, 100 Inha-ro, Michuhol-gu, Incheon, Republic of Korea 22241153@inha.edu
- ² Dept. of Geoinformatic Engineering, Inha University, 100 Inha-ro, Michuhol-gu, Incheon, Republic of Korea *tezid@inha.ac.kr

Keywords: Lightglue, Image Mosaic, Feature Matching, Bundle Adjustment, UAV Image

Abstract

Unmanned Aerial Vehicle (UAV) imagery is playing an important role in various remote sensing applications, including precision agriculture, environmental monitoring, and urban planning. To construct a seamless and geometrically accurate mosaic from multiple overlapping UAV images, it is essential to interpret the camera geometry accurately and extract tiepoints between images reliably. In this study, we focus on evaluating the robustness and effectiveness of the combination of SIFT with LightGlue, a hybrid matching approach that integrates the rotationally invariant properties of SIFT with the contextual matching capabilities of LightGlue. For comparison, we tested two traditional methods, the SIFT with Brute-Force matcher and the SIFT with FLANN matcher, and one AI-based method, the SuperPoint with LightGlue matcher. These matching algorithms were applied to UAV datasets covering both high-texture regions, such as urban environments, and low-texture areas, such as agricultural fields. The performance evaluation was conducted based on several criteria, including the number and spatial distribution of tiepoints, epipolar error, rotational robustness, bundle adjustment stability, and mosaic completeness. Among all methods, the SIFT with LightGlue matcher consistently demonstrated the most reliable performance. This approach not only achieved robust and accurate matching in low-texture and high-rotation scenarios but also led to superior spatial consistency in bundle adjustment and final mosaics, confirming its suitability for practical UAV image mosaicking tasks.

1. Introduction

Unmanned Aerial Vehicle (UAV) imagery is playing an important role in various remote sensing applications, including precision agriculture, environmental monitoring, and urban planning. However, due to the limited field of view of UAV platforms, image mosaicking, which integrates multiple overlapping images into a single seamless composite, is an essential preprocessing step. To achieve precise and gap-free mosaicking, it is critical to accurately interpret the imaging geometry of the camera during acquisition in order to estimate ground coordinates with high accuracy. In photogrammetry, this is typically accomplished through bundle adjustment. In this process, tiepoints, feature points commonly observed between image pairs, are key elements that significantly affect both the accuracy and precision of the adjustment. The accuracy and spatial distribution of tiepoints are critical for stabilizing camera parameter estimation and minimizing geometric distortion in the resulting mosaic. The choice of tiepoint extraction algorithm has a substantial impact on the quality of UAV mosaicking.

Traditionally, descriptor-based feature extraction algorithms such as SIFT, SURF, and ORB combined with Brute-Force or FLANN matcher have been widely used for tiepoint extraction (Zhang et al., 2018). Among these, SIFT has shown favorable performance for UAV imagery acquired from various viewing angles, as it structurally ensures rotational invariance by computing the dominant orientation during feature detection (Lowe, 2004). However, these traditional methods tend to concentrate tiepoints along edges, resulting in an uneven spatial distribution across the image. This limitation becomes more pronounced in textureless regions such as farmlands areas, where reliable tiepoint extraction is particularly challenging (Wu et al., 2021).

Recently, LightGlue has been proposed as a method that employs self-attention and cross-attention mechanisms to learn contextual relationships between feature points and perform precise matching (Lindenberger et al., 2023). LightGlue is typically used in conjunction with SuperPoint, a CNN-based feature detector, and has achieved state-of-the-art results across several benchmarks (Morelli et al., 2024). However, detectors such as SuperPoint are generally robust to translation but relatively vulnerable to rotation and scale variations (Mo and Zhao, 2024). This weakness can lead to matching errors in UAV imagery, where flight directions and camera poses frequently change. In fact, several studies have reported that the SuperPoint with LightGlue combination produces larger geometric errors than SIFT-based methods (Song et al., 2024). Therefore, combining SIFT with LightGlue may offer a promising approach to compensate for the respective weaknesses of each method.

In this study, we apply the SIFT with LightGlue combination to TIN-based UAV image mosaicking algorithm (Yoon and Kim., 2024) and evaluate the robustness of the SIFT with LightGlue by comparing it with both AI-based and traditional matching methods. The experiments were conducted using UAV images acquired over both complex urban environments, which contain various artificial structures and open areas, and low-texture regions such as farmlands. The goal was to analyze the performance of each algorithm in terms of tiepoint extraction and mosaic generation. In addition, considering the characteristics of UAV imaging, we evaluated the matching performance under both nearly non-rotated conditions and extreme cases with nearly 180-degree image rotations. For comparative analysis, we used the previously mentioned SIFT algorithm with Brute-Force and FLANN matchers, as well as the SuperPoint with LightGlue matcher, which is known for its high accuracy among LightGluebased methods.

This paper is structured as follows: we first present the analysis methodology for the mosaicking algorithm and tiepoint extraction performance. We then evaluate the performance at each stage, including tiepoint extraction, bundle adjustment, and image mosaicking. Finally, the main findings are summarized in the conclusion.

2. Methodology

2.1 Mosaicking Process

Figure 1 illustrates the overall workflow of the proposed UAV image mosaicking pipeline. First, the algorithm selects image matching pairs and extracts initial tiepoints. These tiepoints are refined using a relative geometric model to retain only geometrically accurate triplet points, feature points commonly observed between three images (Yoon and Kim., 2023). Bundle adjustment is performed using the selected tiepoints and coplanarity constraints to optimize the camera poses and 3D point coordinates. Finally, using the optimized 3D points, the method corrects image distortions through a TIN (Triangulated Irregular Network)-based image warping technique, and generates a high-resolution, geometrically precise mosaic image.

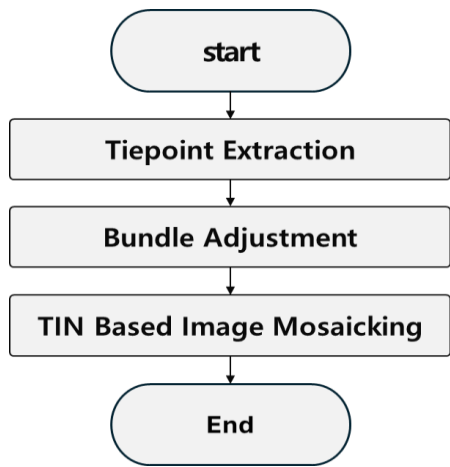


Figure 1. Flowchart of the proposed method

2.2 Evaluation Method for Tiepoint Extraction Performance

Tiepoints are a critical component for performing bundle adjustment and generating image mosaics, as they play a key role in accurately determining the geometric relationships between images. In this study, we focus on evaluating the performance of the hybrid matching method, SIFT with LightGlue, and compare it with traditional approaches (SIFT with Brute-Force, SIFT with FLANN) and deep learning-based methods (SuperPoint with LightGlue), as summarized in Table 1. The performance evaluation is conducted in terms of the number and spatial distribution of triplets, matching accuracy, and robustness to rotation. Emphasis is placed on verifying the performance of the SIFT with LightGlue combination under various conditions.

Test Case	Туре	Detector	Matcher
1	Traditional	SIFT	Brute-Force
2	Traditional	SIFT	FLANN
3	AI-Based	SuperPoint	LightGlue
4	Hybrid	SIFT	LightGlue

Table 1. Matching Algorithm using Experiment

The number of tiepoints is the most fundamental metric for evaluating matching performance, as a higher number of tiepoints provides more observations for subsequent bundle adjustment. In particular, triplets play a crucial role in ensuring geometric consistency. Because they satisfy the epipolar geometry across all three image pairs, triplets serve as a key indicator for accurate bundle adjustment. Accordingly, this study uses both the total number of tiepoints and the number of triplet points as separate evaluation metrics.

In addition to the number of tiepoints, the uniformity of their spatial distribution within each image is also a critical factor in establishing accurate geometry (Vahid Mousavi et al., 2021). To quantitatively evaluate this aspect, each image is divided into a 20×20 grid, and the coverage ratio is computed as the proportion of grid cells containing at least one tiepoint, as defined in Equation (1), where $N_{occ\ grid}$ refers to the number of cells containing tiepoints and $N_{total\ grid}$ to the number of total cells within one image.

Coverage Ratio(%) =
$$\sum \frac{N_{occ\ grid}}{N_{total\ grid}} * 100$$
 (1)

To qualitatively examine how tiepoints are distributed within each image, we visualize the spatial locations of the extracted tiepoints. This analysis focus on evaluating whether tiepoints are evenly distributed not only in high-texture areas such as buildings and roads, but also in low-texture regions with minimal brightness variation, such as within agricultural fields.

Even if a large number of tiepoints are extracted and their distribution is uniform across the image, geometric analysis may still be compromised if the tiepoints are not located at geometrically accurate positions. This is because inaccurate tiepoints can introduce errors in the bundle adjustment process, leading to incorrect estimation of camera poses and 3D scene structure, ultimately degrading the geometric accuracy of the entire image. In this study, epipolar error was used as a quantitative metric to evaluate the geometric accuracy of tiepoints. The epipolar condition is a fundamental condition that describes the geometric relationship between stereo image pairs. In our approach, the fundamental matrix was estimated from the set of tiepoints, and epipolar lines were generated on the right image based on this matrix. The epipolar error was then defined as the perpendicular distance between each corresponding tiepoint and its associated epipolar line.

For matching algorithms applied to UAV imagery, where frequent rotations occur, robustness to rotation is essential. UAV platforms typically capture images in one direction and then rotate nearly 180° to capture the next flight strip in the opposite direction. As a result, image pairs are often composed of one image from one flight strip and one image from an adjacent flight strip and have opposite viewing directions. This characteristic provides a valuable experimental condition for evaluating the rotational robustness of tiepoint matching algorithms.

To analyze this aspect, we categorized the image pairs into two types based on the UAV flight pattern. Intra-strip pairs refer to image pairs captured within the same flight strip and generally exhibit similar viewing directions. In contrast, inter-strip pairs refer to pairs composed of images from adjacent flight strips, which typically have opposite viewing directions due to the platform's rotation between strips.

To quantitatively assess the rotational robustness of each matching algorithm, we measure the number of matches for both intra-strip and inter-strip image pairs. In addition, we conduct a qualitative evaluation by visualizing the matching results for representative scenes that reflect the characteristics of the dataset.

2.3 Evaluation Method for Bundle Adjustment

For precise UAV image mosaicking, accurate estimation of camera parameters and reconstruction of ground coordinates based on geometric alignment between overlapping images is essential. In this study, we evaluated the performance of the bundle adjustment model established through tiepoints using two key indicators: reprojection error and the number of reconstructed 3D ground points.

Reprojection error refers to the distance between the actual tiepoints and the reprojected points when the reconstructed 3D points, obtained through bundle adjustment, are projected back onto the original images. It serves as a primary metric for assessing the precision of camera parameter estimation.

Meanwhile, the reconstructed 3D ground points are derived from overlapping stereo images using the refined tiepoints. The number and spatial distribution of these points are used as qualitative indicators of mosaic quality and geometric stability.

2.4 Evaluation Method for Mosaic quality Performance

The quality of the mosaic was qualitatively evaluated based on visual continuity across image boundaries, the presence or absence of gaps between adjacent images, and the completeness of the mosaic area without missing regions (holes). Specifically, visual inspection was conducted to identify discontinuities, geometric distortions, and inconsistencies along the seams of the mosaic generated by each algorithm, thereby assessing the overall mosaic completeness.

3. Experimental Environment and Dataset

3.1 Experimental Environment

All experiments were conducted on a Windows system equipped with an 11th Gen Intel i7-11700, 32 GB RAM, and an NVIDIA RTX 3070 GPU (24 GB memory). The algorithms were implemented using C++, Python 3.10 and OpenCV 4.5. The LightGlue algorithm was adopted from official GitHub implementation, released in August 2023 (Lindenberger et al., 2023).

3.2 Experimental Dataset

The datasets used in the experiments are summarized in Table 2. Each dataset consists of UAV images with approximately 70 to

80% overlap and can be categorized into two environmental types. The first type is a mixed environment that includes both artificial structures and low-texture areas such as sports fields and grassy regions. The second type is dominated by low-texture areas, such as agricultural fields. Considering these differing texture characteristics, this study quantitatively analyzed tiepoint extraction performance across distinct zones. The objective is to compare algorithm performance under diverse scene conditions and to identify a robust and generalizable tiepoint extraction method applicable to both complex and low-texture environments.

Dataset Name		Dataset 1	Dataset 2	
Flight Type		Fixed Wing	Fixed Wing	
Image Num		60	171	
Image Size		$7,952 \times 5,304$	4,896 ×3,672	
01	End	80%	85%	
Overlap	Side	70%	75%	
GSD		0.0242m	0.0482m	
Characters		Mixed-Texture	Low-Texture	
		Area (e.g.,	Area	
		buildings,	(e.g., rural,	
		ground,etc)	grasslands, etc.)	

Table 2. Dataset Information









(b) Images from Dataset 2 Figure 2. Dataset Example

ID	Matching Algorithm	Feature Num	Tiepoint Num (Total / Triplet)	Coverage Ratio (%) (Total / Triplet)	Epipolar Error (pixel)
	SIFT/Brute-Force	1,788,603	158,919 / 71,260	80.39 / 76.91	1.09
Dataset1	SIFT/FLANN	1,788,603	158,075 / 69,034	81.06 / 77.24	1.13
	Superpoint/LightGlue	230,574	52,341/ 26,286	87.78 / 78.83	1.41
	SIFT/LightGlue	495,504	73,388 / 32,320	90.36 / 83.56	1.20
Dataset2	SIFT/Brute-Force	1,260,069	111,718 / 38,442	42.52 / 31.28	1.01
	SIFT/FLANN	1,260,069	112,067 / 37,843	42.77 / 31.36	1.02
	Superpoint/LightGlue	399,590	81,411/28,003	69.35 / 45.70	1.36
	SIFT/LightGlue	1,129,681	233,102 / 92,094	82.41 / 65.92	1.20

Table 3. Tipoint Extraction Result

4. Experimental Result

4.1 Tiepoint Extraction Result

To evaluate the tiepoint extraction performance of each matching algorithm, we applied the methods to the UAV datasets and assessed them based on the number and spatial distribution of tiepoints and triplet points, epipolar error, and robustness to rotation. Table 3 summarizes the results related to tiepoint quantity, distribution uniformity, and geometric accuracy, while Table 4 presents the evaluation of rotational robustness using intra-strip and inter-strip image pair configurations.

In Dataset 1, the traditional methods, SIFT with Brute-Force and SIFT with FLANN, extracted more keypoints and tiepoints than the LightGlue-based methods (SIFT with LightGlue and Super-Point with LightGlue). However, in terms of coverage ratio, the SIFT with LightGlue outperformed the traditional ones, indicating better spatial uniformity in tiepoint distribution.

Figure 3 visualizes the spatial distribution of tiepoints across the datasets. As shown, traditional methods failed to extract tiepoints in low-texture regions such as sports field interiors or grassy areas, instead concentrating most of the matches along strong linear boundaries or artificial edges. In contrast, LightGlue-based methods produced more evenly distributed tiepoints, even within texture-poor areas. The results in Figure 3 are consistent with the coverage ratio results in Table 3.

This difference of tiepoint extraction in spatial distribution became more pronounced in Dataset 2, which mainly consists of low-texture environments such as agricultural fields. Although the SuperPoint with LightGlue extracted fewer tiepoints overall due to the limited number of keypoints initially detected by SuperPoint, the SIFT with LightGlue method yielded more than twice the number of tiepoints and triplet points compared to traditional methods. Moreover, the coverage ratio was also significantly higher for SIFT with LightGlue.

As shown in Figure 3, the traditional methods tended to extract tiepoints only along strong edges such as field boundaries or ridges, and failed to detect tiepoints in the central low-texture areas of the farmland. On the other hand, LightGlue-based methods were able to extract a dense and spatially uniform set of tiepoints even in these low-texture regions.



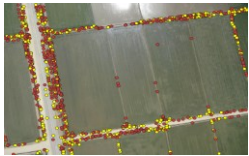




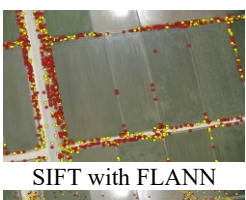


Superpoint with LightGlue SIFT with LightGlue

(a) Results from Dataset 1







Superpoint with LightGlue SIFT with LightGlue (b) Results from Dataset 2

Figure 3. Tiepoint/Triplet Distribution Result *Red Point : Tiepoint, Yellow Point : Triplet

Building on the previous findings regarding quantity and distribution, we further analyzed the geometric accuracy of the extracted tiepoints. A more comprehensive evaluation of tiepoint extraction must also consider the epipolar error, which we used to assess geometric accuracy, as presented in Table 1.

The results show that traditional methods consistently produced lower epipolar errors across all datasets compared to LightGluebased methods. In particular, the AI-based SuperPoint with LightGlue exhibited relatively high errors, with differences exceeding 0.3 pixels on average compared to traditional methods. On the other hand, the SIFT with LightGlue showed only a minor difference of approximately 0.1 pixels, indicating negligible degradation in accuracy.

These findings are consistent with previous studies (Ye et al., 2023; Wang et al., 2023; Luo et al., 2024), which have also reported that traditional algorithms tend to yield higher geometric accuracy than LightGlue-based approaches.

Detect	Matching Algorithm	Total Inlier Num		Average Inlier Num	
Dataset ID		Intra Strip Pair	Inter Strip Pair	Intra Strip Pair	Inter Strip Pair
Dataset 1	SIFT/ Brute-Force	247,806	136,188	4,589	2,522
	SIFT/ FLANN	241,326	133,002	4,469	2,466
	Superpoint/ LightGlue	94,230	1,350	1,745	25
	SIFT/ LightGlue	225,072	89,802	4,168	1,663
Dataset 2	SIFT/ Brute-Force	115,280	71,808	655	408
	SIFT/ FLANN	114,048	71,456	648	406
	Superpoint/ LightGlue	129,008	2,112	733	12
	SIFT/ LightGlue	355,520	95,920	2,020	545

Table 4. Matching performance by rotation.

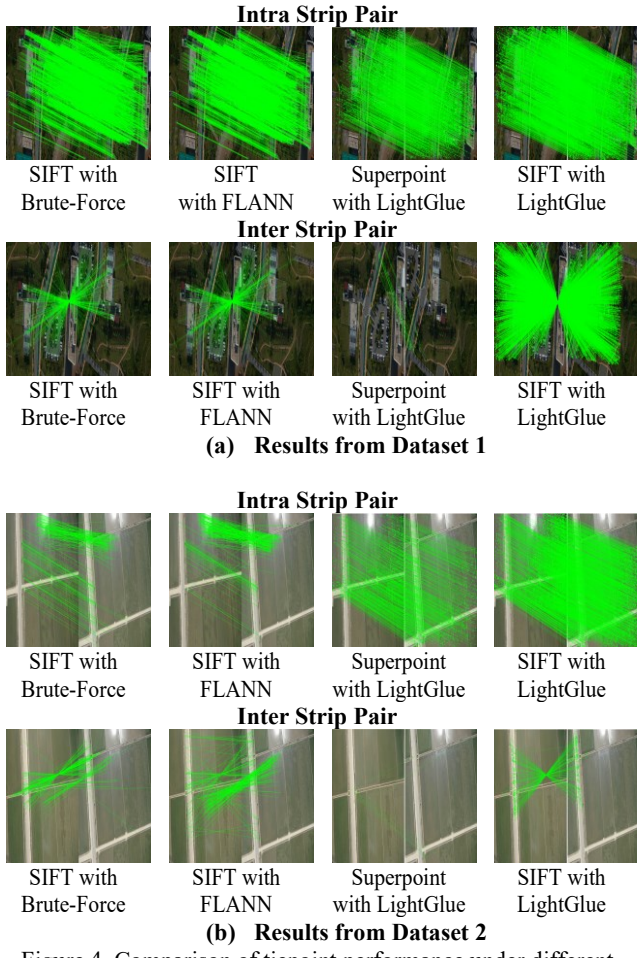


Figure 4. Comparison of tiepoint performance under different rotation conditions. The figure shows intra-strip matching results (approx. 0° difference) and inter-strip matching results (approx. 180° rotation) for each algorithm.

In UAV imagery, significant variations in imaging direction frequently occur between flight strips. Therefore, the rotational robustness of tiepoint matching algorithms is a critical factor in determining their practical applicability. Table 4 presents the results of matching performance under different rotational conditions by comparing the number of RANSAC-based inliers between intrastrip pairs (with approximately 0° rotation difference) and interstrip pairs (with approximately 180° rotation difference).

The analysis shows that matching algorithms using SIFT experienced some performance degradation in inter-strip matching compared to intra-strip matching. However, they consistently maintained more than 400 inliers across all datasets, demonstrating strong robustness to rotational variation.

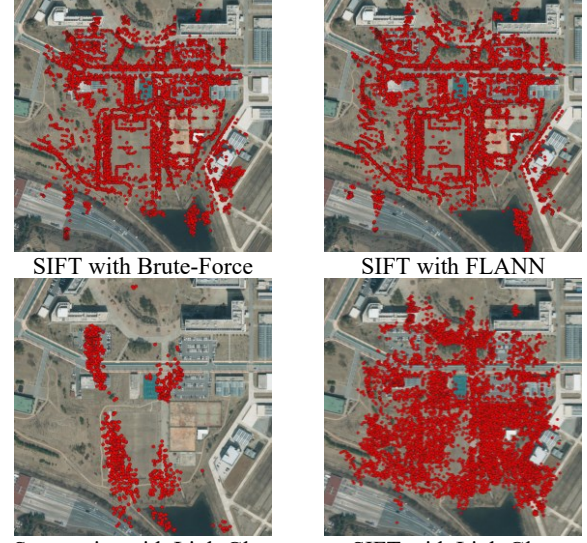
In contrast, SuperPoint with LightGlue exhibited a substantial drop in the number of tiepoints when transitioning from intrastrip to inter-strip matching. This trend is also qualitatively evident in Figure 4, where the SuperPoint with LightGlue combination shows significantly lower performance than SIFT-based algorithms in both the number of tiepoints and geometric accuracy under inter-strip conditions.

These results indicate that the SuperPoint with LightGlue combination is highly vulnerable to large rotational changes, such as 180°, leading to severe degradation in matching performance.

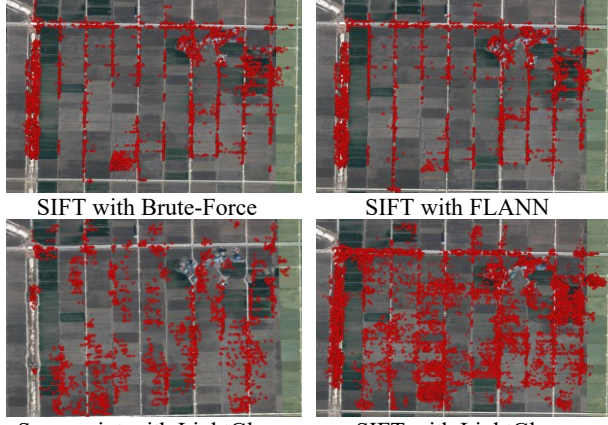
4.2. Bundle Adjustment Result

Dataset ID	Matching Algorithm	Reprojection Error (pixel)	3D Point Num
	SIFT/ Brute-Force	2.22	13,789
	SIFT/ FLANN	2.23	13,673
Dataset1	SIFT/ LightGlue	2.25	10,128
	Superpoint/ LightGlue	3.35	957
	SIFT/ Brute-Force	1.83	9,997
D-442	SIFT/ FLANN	1.84	8,953
Dataset2	SIFT/ LightGlue	1.88	19,176
	Superpoint/ LightGlue	3.33	3,549

Table 5. Bundle Adjustment Result.



Superpoint with LightGlue SIFT with LightGlue
(a) Results from Dataset 1



Superpoint with LightGlue

(b) Results from Dataset 2

Figure 5. 3D Point Distribution by Algorithm.

Bundle adjustment was performed using the tiepoints extracted by each matching algorithm, and the results were analyzed both quantitatively and qualitatively. The performance of the bundle adjustment was assessed based on the reprojection error as well as the quantity and spatial distribution of the reconstructed 3D points, as summarized in Table 5.

In terms of reprojection error, SIFT with Brute-Force showed the highest accuracy in both Dataset 1 and Dataset 2, yielding the lowest error values. The other traditional method, SIFT with FLANN, also achieved a comparable level of accuracy. In contrast, the SuperPoint with LightGlue resulted in a significantly higher reprojection error, increasing by more than 1 pixel compared to the traditional methods. Although SIFT with LightGlue produced slightly higher reprojection errors than the traditional methods, the difference from SIFT with Brute-Force—the best-performing method—was within 0.03 pixels, indicating that the actual performance degradation was negligible.

Regarding the number of 3D points, the LightGlue-based methods produced fewer 3D points than the traditional methods in Dataset 1, with SuperPoint with LightGlue generating the fewest. However, as shown in Figure 5, the 3D points generated by the traditional methods were mostly concentrated along high-contrast edges, such as field boundaries or lines on the sports ground. In low-texture areas, such as the center of the sports field, few or no 3D points were generated. This result is consistent with the previously observed tiepoint distribution patterns.

The SuperPoint with LightGlue method yielded highly irregular results, with 3D points either clustered along straight lines or sparsely distributed in only limited regions, suggesting that bundle adjustment was likely not performed successfully. This can be attributed to the lack of sufficient and accurate tiepoints between inter-strip image pairs, as previously identified in the rotational robustness analysis. On the other hand, the SIFT with LightGlue method produced the most uniformly distributed 3D points among all tested combinations, with points also appearing in low-texture areas such as the central region of the sports field.

In Dataset 2, SIFT with LightGlue generated more than twice as many 3D points as the traditional methods. Moreover, unlike the traditional methods, which produced 3D points primarily along boundaries and edges, the LightGlue-based method resulted in a more widespread distribution, extending into interior regions of agricultural fields. A similar trend was partially observed in the SuperPoint with LightGlue results as well.

4.3. Mosaic Result







SIFT with FLANN



SIFT with LightGlue SIFT with LightGlue
(b) Mosaic Results from Dataset2
Figure 6. Final Mosaic Result by Algorithm.

For each algorithm, tiepoints were extracted and refined through bundle adjustment to generate precise 3D ground coordinates, which were then used to create mosaics. The resulting mosaics were qualitatively evaluated based on visual completeness and alignment gaps. Figure 6 presents the mosaic output generated by each algorithm.

In Dataset 1, all algorithms except for SuperPoint with LightGlue successfully produced seamless mosaics without noticeable gaps. In contrast, the SuperPoint with LightGlue combination failed to achieve stable bundle adjustment, leading to poor geometric alignment between images. As a result, geometric distortions and mosaic gaps were observed in the output.

In Dataset 2, due to the overall low image quality and weak texture characteristics, both traditional methods and SuperPointbased algorithms exhibited significant mosaic failures or missing regions. On the other hand, SIFT with LightGlue succeeded in generating a stable and extensive mosaic, outperforming other methods under the same conditions.

These results are consistent with the earlier analyses of tiepoint extraction and bundle adjustment accuracy, confirming that the SIFT with LightGlue delivers the most reliable mosaic quality among the evaluated algorithms.

5. Conclusion

In this study, we focused on evaluating the effectiveness of the SIFT with LightGlue combination for tiepoint extraction, bundle adjustment, and mosaic generation in UAV imagery, and compared the performance with traditional and deep-learning-based methods. Experimental results revealed that SIFT with LightGlue achieved the most uniform spatial distribution of tiepoints, even

in low-texture regions, despite extracting fewer tiepoints overall. This led to superior spatial coverage compared to other methods.

In terms of geometric accuracy, SIFT with LightGlue achieved a level of epipolar error comparable to traditional SIFT-based methods. The SIFT with LightGlue also exhibited stable matching performance under nearly extreme rotational conditions. These results demonstrate the robustness of the SIFT with LightGlue to challenging geometric variations.

Although the reprojection error during bundle adjustment was slightly higher, the SIFT with LightGlue yielded the most evenly distributed 3D ground points and enabled stable adjustments even in low-texture areas. Final mosaic results further confirmed this pattern, with the SIFT with LightGlue successfully generating seamlessly aligned mosaics, outperforming other methods in terms of mosaic completeness.

Overall, the SIFT with LightGlue combination demonstrated the best balance of accuracy, spatial coverage, and robustness, making it the most reliable algorithm for UAV image alignment and mosaicking. Future work should aim to extend the applicability of this approach to more diverse and challenging environments, including large-scale datasets and densely built-up urban areas.

Acknowledgements

This work is supported by the Korea Agency for Infrastructure Technology Advancement (KAIA) grant funded by the Ministry of Land, Infrastructure and Transport (Grant RS-2022-00155763).

References

Lindenberger, P., Sarlin, P.E., Pollefeys, M., 2023: LightGlue: local feature matching at light speed. *Proc. IEEE/CVF Int. Conf. Comput. Vision (ICCV)*, 17627–17638. doi.org/10.48550/arXiv.2306.13643.

Lindenberger, P., Sarlin, P.-E., Pollefeys, M., 2023. *LightGlue – Local Feature Matching at Light Speed*. GitHub repository, https://github.com/cvg/LightGlue (accessed 7 Jul 2025).

Lowe, D.G., 2004: Distinctive image features from scale-invariant keypoints. *Int. J. Comput. Vision*, 60, 91–110. doi.org/10.1023/B:VISI.0000029664.99615.94.

Luo, Q., Zhang, J., Xie, Y., Huang, X., Han, T., 2024: Comparative analysis of advanced feature matching algorithms in challenging high spatial resolution optical satellite stereo scenarios. *Proc. IEEE Int. Geosci. Remote Sens. Symp. (IGARSS)*, 2645–2649. doi.org/10.1109/IGARSS53475.2024.10641727.

Mo, H., Zhao, G., 2024: RIC-CNN: rotation-invariant coordinate convolutional neural network. *Pattern Recognit.*, 146, 109994. doi.org/10.1016/j.patcog.2023.109994.

Morelli, L., Ioli, F., Maiwald, F., Mazzacca, G., Menna, F., Remondino, F., 2024: Deep-image-matching: a toolbox for multiview image matching of complex scenarios. *Int. Arch. Photogramm. Remote Sens. Spatial Inf. Sci.*, XLVIII-2/W4-2024, 309–316. doi.org/10.5194/isprs-archives-XLVIII-2-W4-2024-309-2024.

Mousavi, V., Varshosaz, M., Remondino, F., 2021. Evaluating tie points distribution, multiplicity and number on the accuracy of UAV photogrammetry blocks. *Int. Arch. Photogramm.*

Remote Sens. Spatial Inf. Sci., XLIII-B2-2021, 39–46. doi.org/10.5194/isprs-archives-XLIII-B2-2021-39-2021.

Song, S., Morelli, L., Wu, X., Qin, R., Albanwan, H., Remondino, F., 2024: Evaluating learning-based tie point matching for geometric processing of off-track satellite stereo. *Int. Arch. Photogramm. Remote Sens. Spatial Inf. Sci.*, XLVIII-2-2024, 393–400. doi.org/10.5194/isprs-archives-XLVIII-2-2024-393-2024.

Wang, Y., Zhou, K., Chen, P., Zhang, H., 2023: Accuracy comparison between handcrafted and deep learning-based local features in large-scale UAV 3-D reconstruction. *ISPRS J. Photogramm. Remote Sens.*, 198, 124–138. doi.org/10.1016/j.isprsjprs.2023.03.004.

Wu, H., Li, X., Zhang, H., Sun, Y., Zhao, M., 2021: Using information content to select keypoints for UAV image matching. *Remote Sens.*, 13, 1302. doi.org/10.3390/rs13071302.

Ye, J., Li, S., Liu, B., Chi, H., 2023: Benchmarking learning-based and traditional feature matching for UAV photogrammetry. *Remote Sens.*, 15(8), 2105. doi.org/10.3390/rs15082105

Yoon, S.J., Kim, T., 2024: Seamline optimization based on triangulated irregular network of tiepoints for fast UAV image mosaicking. *Remote Sens.*, 16, 1738. doi.org/10.3390/rs16101738.

Yoon, S.J., Kim, T., 2023: Fast UAV Image Mosaicking by a Triangulated Irregular Network of Bucketed Tiepoints. *Remote Sens.*, 15, 5782. doi.org/10.3390/rs15245782.

Zhang, W., Li, X., Yu, J., Kumar, M., Mao, Y., 2018: Remote sensing image mosaic technology based on SURF algorithm in agriculture. *EURASIP J. Image Video Process.*, 2018, 1–9. doi.org/10.1186/s13640-018-0323-5.